

Evaluation of 2D spatially selective MR spectroscopy using parallel excitation at 7 T

Gopesh Patel¹, Martin Haas², Niravkumar Darji¹, Oliver Speck^{1,3,4,5}

¹Department of Biomedical Magnetic Resonance, Institute for Experimental Physics, Otto-von Guericke University Magdeburg, Leipzigerstr. 44, 39120 Magdeburg, Germany; ²Medical Physics, Department of Radiology, University Medical Center Freiburg, Breisacherstr. 60a, 79106 Freiburg, Germany; ³German Center for Neurodegenerative Diseases (DZNE), Site Magdeburg, Leipzigerstr. 44, 39120 Magdeburg, Germany; ⁴Leibniz Institute for Neurobiology, Brenneckestr. 6, 39118 Magdeburg, Germany; ⁵Center for Behavioral Brain Sciences, Universitaetsplatz 2, 39106 Magdeburg, Germany

Correspondence to: Gopesh Patel. Leipzigerstr. 44, 39120 Magdeburg, Germany. Email: patelgopesh@gmail.com.

Background: In this work, two-dimensional (2D) spatially selective magnetic resonance spectroscopy (MRS) was evaluated in both phantom and human brain using 8-channel parallel excitation (pTX) at 7 T and compared to standard STEAM.

Materials and methods: A 2D spiral excitation k-space trajectory was segmented into multiple individual segments to increase the bandwidth. pTX was used to decrease the number of segments by accelerating the trajectory. Different radio frequency (RF) shim settings were used for refocusing, water suppression and fat saturation pulses.

Results: Phantom experiments demonstrate that, although segmented 2D excitation provided excellent spatial selectivity and spectral quality, STEAM outperformed it in terms of outer volume suppression with 0.6% RMSD compared to 1.7%, 2.5%, 3.9% and 5.5% RMSDs for acceleration factors of R=1, 2, 3 and 4, respectively. Seven major metabolites [choline (Cho), creatine (Cr), phosphocreatine (PCr), glutamate (Glu), glutamine (Gln), glutathione (GSH) and N-acetylaspartate (NAA)] were detected with sufficient accuracy [Cramér-Rao lower bounds (CRLBs) <20%] from the in vivo spectra of both methods. Conservative RF power limits resulted in reduced SNR for 2D selective MR spectra (SNR 131 and 82 for R=1 and 2, respectively) compared to the reference STEAM spectrum (SNR 199).

Conclusions: Single voxel spectra acquired using 2D selective MRS with and without pTX showed very good agreement with the reference STEAM spectrum. Efficient SAR management of the 2D selective MRS sequence would potentially improve the SNR of spectra.

Keywords: Parallel excitation (pTX); radio frequency (RF) shimming; segmented two-dimensional (2D) excitation; single voxel spectroscopy

Submitted Dec 04, 2014. Accepted for publication Feb 13, 2015.

doi: 10.3978/j.issn.2223-4292.2015.03.05

View this article at: <http://dx.doi.org/10.3978/j.issn.2223-4292.2015.03.05>

Introduction

In conventional magnetic resonance imaging and spectroscopy, a radio frequency (RF) pulse with a specific frequency bandwidth is applied while a constant magnetic field gradient is switched on. From the Fourier perspective, the applied gradients during the RF pulse map a trajectory

in k-space (excitation k-space trajectory). As the trajectory is being mapped out, the RF pulse provides a weighting function to the trajectory. For small tip-angles (STAs), the resulting slice profile can be approximated by the Fourier transform of the weighted k-space distribution (1). Thus, a rectangular slice profile produced by slice-selective excitation can be visualized as a sinc RF pulse weighting the

slice axis of the trajectory while a constant slice selection gradient is switched on. Because the excited volume is confined to a single slice, it is referred to as one dimensional (1D) spatially selective excitation (SSE).

Spatial selectivity in the two most commonly used single voxel magnetic resonance spectroscopy (MRS) methods, stimulated echo acquisition mode (STEAM) (2) and point resolved spectroscopy (PRESS) (3) is achieved by a combination of three slice-selective RF pulses in mutually orthogonal planes. These methods are referred to as 1D selective MRS methods. Transverse magnetization outside the area of intersection of these three orthogonal slices is subsequently dephased by spoiler gradients to localize the generated signal in the volume of intersection. Therefore, the excited volume always remains cuboidal in shape. However, anatomical structures are composed of different types of tissues which are complex in shape. This leads to contamination of the spectrum because of inclusion of metabolites from outside the target anatomy. To avoid these partial volume artifacts in the spectrum, a compromise in the coverage of the target region is required, which may lead to loss of sensitivity for important metabolites of interest.

Multidimensional SSE can effectively mitigate the problem of partial volume artifacts by designing tailored RF pulses to excite any arbitrarily shaped voxel (1). This is achieved by traversing a multidimensional excitation k-space trajectory by time-varying gradients in two or more dimensions during the RF excitation. As the trajectory now becomes variable due to time-varying gradients, the RF pulse must be calculated accordingly for proper weighting. Two-dimensional (2D) SSE is accomplished by traversing a 2D trajectory weighted by a 2D RF excitation pulse designed to excite magnetization in an arbitrarily shaped region within a plane and suppress it in the surrounding area. The resulting volume is localized in a through-plane dimension by 1D selective refocusing. Because traversal within a 2D trajectory takes longer than within a 1D trajectory, and given the hardware constraints of a gradient system, a 2D RF pulse can be long (tens of milliseconds) compared with a 1D slice-selective RF pulse. RF pulses of such length are susceptible to off-resonance and relaxation effects and therefore unsuitable for use in short echo time (TE) spectroscopic applications. Moreover, MRS requires broad bandwidth RF excitation pulses to effectively excite a broad range of metabolites of interest. However, because of the long duration and consequently short bandwidth, such 2D RF pulses are

unfeasible for spectroscopic applications.

To increase the bandwidth of multidimensional RF pulses and reduce TE, the excitation k-space trajectory can be segmented into multiple smaller segments wherein each segment is traversed in successive acquisitions until the desired excitation k-space is covered (4). Signal acquisition can start immediately after a single refocusing pulse following a 2D RF pulse segment. The resulting spectrum from the target voxel is the complex sum of signals acquired from all segments of the trajectory. Although, the linearity of the Bloch equation for trajectory segments is assured only in the STA regime (flip angle of 30° or less), it continues to hold well for flip angles up to 90° (5), which is a prerequisite to obtain the maximum signal-to-noise ratio (SNR).

Recent studies have shown feasibility of 2D selective MRS on 3 T scanners using a circularly polarized (CP) (single transmit channel) coil (6,7). Parallel excitation (pTX) with multiple independent transmit channels, each with its distinct spatial B1 profile, offers additional degrees of freedom which can be used to shorten the duration of multidimensional RF pulses further by substituting gradient encoding with B1 encoding, increase spatial resolution and control RF power deposition (8,9). In combination with segmentation, pTX can be used to reduce the number of segments of the excitation k-space trajectory by accelerating the trajectory. This has been shown for various 2D trajectories in phantom studies using an 8-channel transmit body coil at 3 T (10). MRS at high field strength (>3 T) has the inherent advantage of providing improved SNR and spectral resolution. However, no *in vivo* pTX MRS study is available yet. The goal of this study was to evaluate the performance of 2D selective MRS accelerated by pTX in both phantom and human brain using an 8-channel transmit head coil on a 7 T scanner and compare the results with the standard STEAM. The comparison focused on the spatial and spectral selectivity of the two methods.

Materials and methods

All experiments were performed on a 7 T whole body human scanner (Siemens Healthcare, Erlangen, Germany) with an SC72A gradient system capable of producing a maximum amplitude of 70 mT/m and a maximum slew rate of 200 mT/m/s. The scanner is equipped with an 8-channel transmit array driving eight independent RF power amplifiers (Stolberg HF Technik, Stolberg, Germany) each capable of transmitting a maximum of 1 kW. For both transmission and reception, an 8-channel transceiver head

coil in a classical loop design was used (Rapid Biomedical, Rimpär, Germany).

Spatial target pattern

A rectangular target was chosen for 2D selective MRS to enable direct comparison of its spectra with the STEAM spectrum, as STEAM can only excite cuboid voxels. The complex 2D target magnetization pattern with uniform flip angle and phase distribution was defined in the transverse plane on a 64×64 Cartesian grid. The 2D target magnetization pattern measured 2×2 cm² and was oriented in the non-selective dimension by a refocusing pulse of 1 cm slice thickness. A standard STEAM sequence was also used with equivalent voxel dimensions for comparison with the 2D selective MRS sequence. The 2D field of excitation (FOX) measured 16×16 and 20×20 cm² for phantom and *in vivo* experiments, respectively. The in-plane resolution of the target measured 2.5 and 3.125 mm for phantom and *in vivo* experiments, respectively. The target pattern was convolved with a Gaussian kernel of size 3×3 and standard deviation of 0.6, resulting in a window size of 2 pixels to avoid ringing artifacts.

Gradient trajectory and RF pulse design

The complex transverse magnetization $M_{target}(x)$ generated by a single shot multidimensional SSE from an array of N transmit channels can be described in the small tip angle (STA) regime by (11):

$$M_{target}(x) = i\gamma M_0 \sum_{n=1}^N S_n(x) \int_0^T B_{1,n}(t) \exp(ix \cdot k(t)) dt \quad [1]$$

where γ is the gyromagnetic ratio, M_0 is the equilibrium magnetization, $S_n(x)$ is the transmit sensitivity of the n^{th} channel, $B_{1,n}(t)$ is the corresponding RF pulse and $k(t)$ is the excitation k-space trajectory generated by simultaneous action of the RF pulse and gradient shape of duration T . Eq. [1] was discretized and the resultant linear system was solved in image space (12) to minimize the residual error by an iterative conjugate gradient least squares algorithm with Tikhonov regularization (13) using the following equation:

$$\text{argmin}_b \|Ab - m\|_w^2 + \beta \|b\|^2 \quad [2]$$

where A is the system matrix containing the excitation k-space trajectory weighted by each channel's transmit sensitivity, b is a vector containing individual RF pulses for each transmit channel, m is a vector containing the desired spatial target pattern, W is a diagonal matrix that specifies a

mask for the spatial target pattern and β is a regularization parameter to control total RF power at the cost of target fidelity. As a single shot trajectory leads to unacceptably long pulse duration and thus low spectral bandwidth, the trajectory was divided into K gradient balanced segments (4). Each segment thus resulted in eight individual RF pulses for each transmit channel with a corresponding gradient segment. The target magnetization distribution $M_{target}(x)$ was produced by the addition of complex transverse magnetization distributions $M_s(x)$ generated by each RF segment s in the STA regime as follows:

$$M_{target}(x) = \sum_{s=1}^K M_s(x) \quad [3]$$

An Archimedean spiral excitation k-space trajectory was used for 2D experiments (14). Design constraints were placed on the trajectory so that slew rate and amplitude limits for the gradient system were not violated at any time point. The spiral trajectory was calculated on a 64×64 grid over 3,000 trajectory points and required 32 revolutions spiraling from the edge of k-space inwards to the center of k-space for full sampling of the FOX. Revolutions were segmented such that each segment spiraled inwards one revolution measuring 940 μ s with a total pulse length of 30 ms. Spiral-in trajectory was chosen over spiral-out as the former is inherently self-refocused due to ending in the center of the excitation k-space (1). Incorporation of individual channel B1 maps in the RF pulse design allowed for an undersampling of the excitation trajectory via B1 encoding (acceleration of trajectory) resulting in a reduction of the overall trajectory length and thereby reducing the total number of segments. The pTX acceleration factor (R) was defined such that, for example $R=2$, when applied to a fully sampled trajectory consisting of 32 segments, would reduce the number of segments to 16 while maintaining the segment length identical to the unaccelerated case.

A gradient trajectory and RF pulse design tool with a graphical user interface was implemented in MATLAB (Mathworks Inc., Natick, MA, USA). The tool allows the user to load B1 sensitivities and an arbitrary spatial target pattern. The user needs to specify the FOX, target grid size, desired flip angle, gradient limits, number of trajectory segments and acceleration factor. The generated RF pulse and gradient trajectory segments can be directly exported to the scanner to be used by the sequence. A Bloch simulator was also incorporated in the pulse design tool to enable visualization of the target pattern produced by the designed RF pulses on-resonance and also at different off-resonance frequencies for bandwidth calculations.

B1 mapping and RF shimming

In a first step, the relative phases between the transmit channels were determined to generate maximum signal in the coil center by constructive interference resembling the quadrature mode of a CP coil (CP excitation mode). B1 phase maps were calculated (15) from low flip angle gradient echo (GRE) images (TE 3.6 ms, TR 60 ms, flip angle 15°, matrix size 64×64 and slice thickness 10 mm) acquired by transmitting the RF pulse individually on each transmit channel in consecutive scans while the signal was received on all receive channels. In a second step, to calculate the flip angle map for each channel, a separate sequence based on a pre-saturated Turbo FLASH (TFL) was used (TE 3 ms, TR 8 s, matrix size 64×64 and slice thickness 10 mm) (16). A slice-selective sinc pre-saturation pulse (flip angle 90°) was applied consecutively on each transmit channel followed by a TFL train of low flip angle pulses (flip angle 8°) simultaneously on all transmit channels, in the pseudo quadrature mode, to encode the longitudinal magnetization while the received signal was sampled on all receive channels. A reference image was also acquired in the same measurement by switching off the pre-saturation pulse and CP mode excitation. The resulting raw data were smoothed by a Hanning filter prior to image reconstruction. A flip angle map for each transmit channel was calculated from the ratio of the signal intensities of the pre-saturated channel image to the reference image assuming negligible T1 effects. Complex B1 maps were created by merging the flip angle maps with relative phase maps. Complex RF shim weights containing optimized amplitude scaling factors and phases for each transmit channel were calculated using the vendor-provided magnitude least squares algorithm (17). In the case of global RF shim mode, the complex RF shim weights were calculated for the entire selected slice while in the case of local RF shim mode, the complex RF shim weights were calculated for only a smaller region of interest within the selected slice. Using local RF shimming, improved RF homogeneity over the region of interest can be obtained as homogenization of smaller area reduces the constraint on the optimization process and therefore better homogeneity can be achieved compared to global RF shimming.

B0 shimming

Higher order B0 shimming was carried out to shim the target excitation volume. B0 field maps were calculated from dual-echo GRE images (TE1 4.08 ms, TE2 5.10 ms, TR 1 s,

flip angle 15°, matrix size 96×96 and slice thickness 4 mm). Optimized B0 shim fields were calculated from these field maps to improve the B0 field homogeneity locally over the target excitation volume. An identical B0 shim setting was applied for both the reference STEAM and 2D selective voxel.

Imaging localization

The standard STEAM sequence was modified by appending the phase encoding and readout modules to measure an image of the voxel (TE 15 ms, TM 15 ms, flip angle 90°, TR 5 s, matrix size 128×128 and slice thickness 10 mm). To measure spatial selectivity of the segmented 2D RF pulses, a fully relaxed modified spin echo (SE) sequence was used (TE 15 ms, TR 5 s, flip angle 30°, matrix size 128×128 and slice thickness 10 mm). The excitation module of the SE sequence (RF pulse and slice selection gradient) was replaced by the pTX module (segmented 2D RF pulse with a corresponding gradient segment) with a unique segment running successively in a multi-average acquisition. The target localization image was produced by summing the complex images created by each segment. Imaging STEAM localization and SE sequences were not applicable *in vivo* due to their long scan times. Therefore, for segmented 2D excitation, an additional modified 3D GRE sequence was implemented for *in vivo* experiments with a pTX module replacing the standard excitation module (TE 4.1 ms, TR 10 ms, matrix size 64×64 and slice thickness 10 mm) and the whole 3D dataset was acquired in a multi-average acquisition. The flip angle was scaled down to 3° to avoid T1 saturation effects due to short TR.

Localized MRS

For 1D selective MRS measurements, the standard STEAM sequence was used in local RF shim mode (TE 15 ms, TM 15 ms and flip angle 90°) (18). The 2D selective MRS sequence (Figure 1) was designed based on a modified spin echo type with a segmented 2D RF pulse followed by a locally RF shimmed refocusing pulse in the non-selective dimension (TE 9.5 ms, excitation flip angle 30° and refocusing flip angle 180°). WET water suppression was performed in both MRS sequences in local RF shim mode (19). Additionally, four globally RF shimmed pre-saturation bands (two each in sagittal and coronal orientations with slice thickness of 30 mm, saturation pulse flip angle of 90° and carrier frequency centered at fat resonance) were used in the

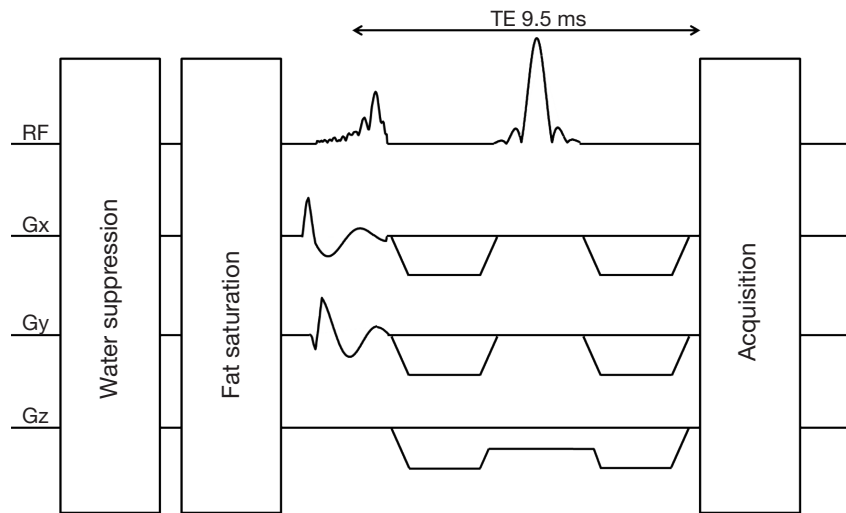


Figure 1 Pulse sequence diagram of the 2D selective MRS sequence with segmented spiral trajectory. Only one segment is shown in the figure. The sequence uses dynamic RF shim settings (fat saturation pulses use global RF shim mode, water suppression pulses and refocusing pulse use local RF shim mode). 2D, two-dimensional; MRS, magnetic resonance spectroscopy; RF, radio frequency.

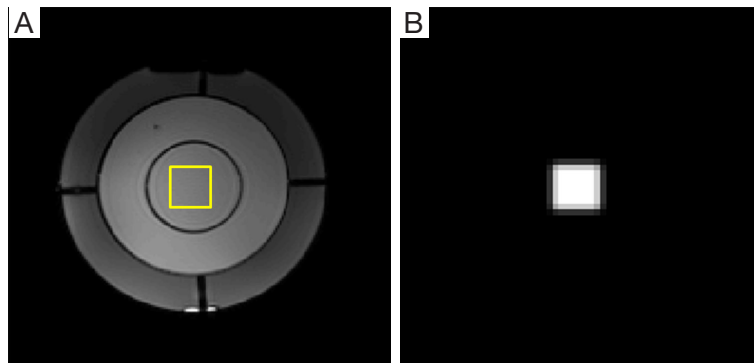


Figure 2 Axial localizer image of the oil-gel-metabolite phantom displaying the location of excitation target in yellow (A) and simulated spatial target pattern (B).

case of 2D selective MRS to avoid lipid contamination in the spectra (20). The spatial fat saturation pulses produced maximal phase dispersion across the saturation bands and were followed by strong spoiler gradients placed along the phase and frequency encoding axes to further suppress the residual transverse magnetization. All spectroscopic measurements had a common TR of 8 s, 2,048 points, 64 averages (2 repetitions per segment for R=1 and 4 repetitions per segment for R = 2), with a total measurement time of 8 min 32 s, carrier frequency centered at -2.2 ppm, and an acquisition bandwidth of 2,800 Hz. *In vivo* spectral analysis was performed using LCModel (21). Basis sets were simulated using VESPA (22).

Phantom experiments

A cylindrical phantom was used to compare the spatial localization of the 2D selective MRS sequence with the standard STEAM sequence. The phantom was constructed of three concentric cylinders made of acrylic glass. *Figure 2A* shows the axial localizer image of the phantom along with the rectangular target superimposed on it. The outermost cylinder (outer diameter =14 cm, inner diameter =13.5 cm) contained 770 mL sunflower oil to emulate the extracranial fat in the human head. The middle cylinder (outer diameter =10 cm, inner diameter =9.6 cm) containing 465 mL deionized water with 1% agarose gel was placed

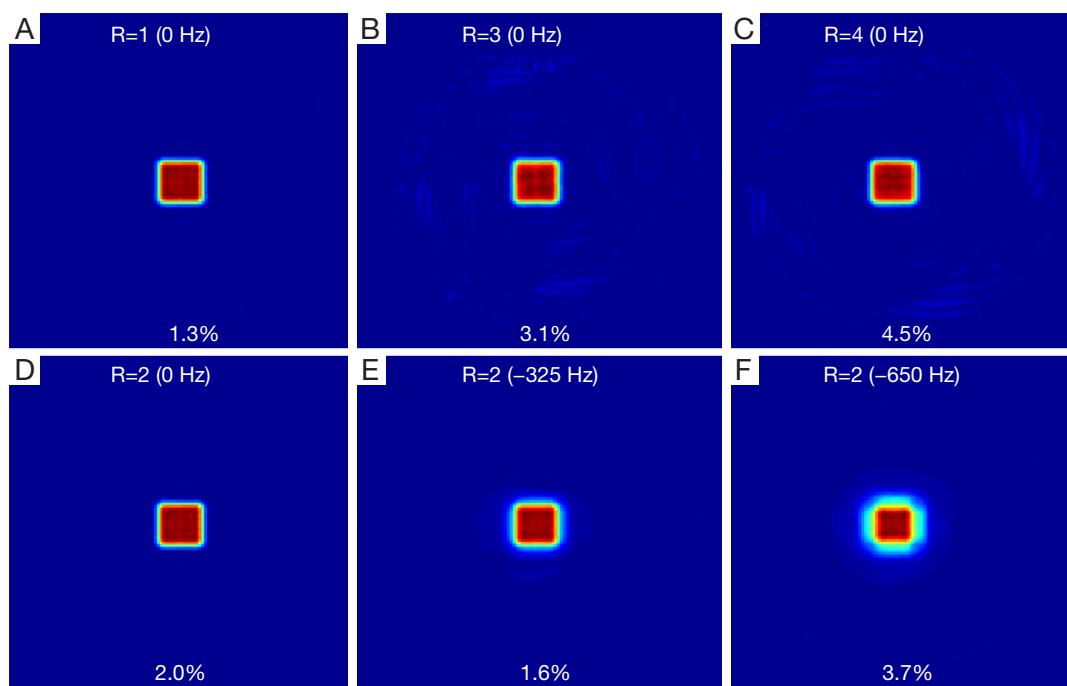


Figure 3 Bloch simulations of the transverse magnetization at on-resonance (0 Hz) for acceleration factors of R=1 (A), R=2 (D), R=3 (B), R=4 (C) and at -325 Hz (E) and -650 Hz (F) off-resonance for R=2. Root-mean-square deviation values are shown at the bottom of the images.

solely to provide the support to the innermost and outermost cylinders, but also helped to test the efficacy of water suppression. The innermost cylinder (outer diameter =5 cm, inner diameter =4.7 cm) contained 55 mL solution of citrate (Cit; resonant frequencies of 2.5-2.7 ppm) and lactate (Lac; resonant frequencies of 1.3 and 4.1 ppm) (23) metabolites with a concentration of 0.1 mmol/L. The target was placed in the innermost cylinder so that ideally only Lac and Cit signals would be excited while completely suppressing the fat from the outermost cylinder.

In vivo experiments

Due to the unavailability of a suitable SAR simulation model for the volunteers recruited in this study, the actual local RF power absorption values could not be modeled. To ensure compliance with the IEC guidelines on SAR, conservative RF power (total forward-going) limits of 0.15 W (averaged over 6 min) and 0.30 W (averaged over 10 s) per channel were derived assuming the worst-case scenario that electric fields of all RF channels add up constructively in all positions in the head (24). The RF output power of each of the eight RF amplifiers was continuously monitored with an

8-channel RF power monitoring and supervision unit. If any of these limits were violated, the system would immediately disable all RF power amplifiers and terminate the pulse sequence. The minimum achievable TR was restricted to 8 s for 2D selective MRS and 5 s for STEAM for *in vivo* experiments because of conservative RF power limits due to pTX selective excitation/RF shimming. The study was approved by the local institutional review board. All five volunteers (healthy male aged between 20 to 30 years) had provided written consent. Representative results for only one volunteer are shown.

Results

Phantom experiments

As the direct calculation of bandwidth was not possible for segmented 2D RF pulses, Bloch simulations of target transverse magnetization at on-resonance and at different off-resonance frequencies were carried out. Assuming the relevant frequency range for major metabolites of interest to be up to -4.4 ppm (~1,300 Hz), rotational symmetry of the spiral trajectory allowed the resonance frequency of segmented 2D RF pulses to be set to the center of the spectral

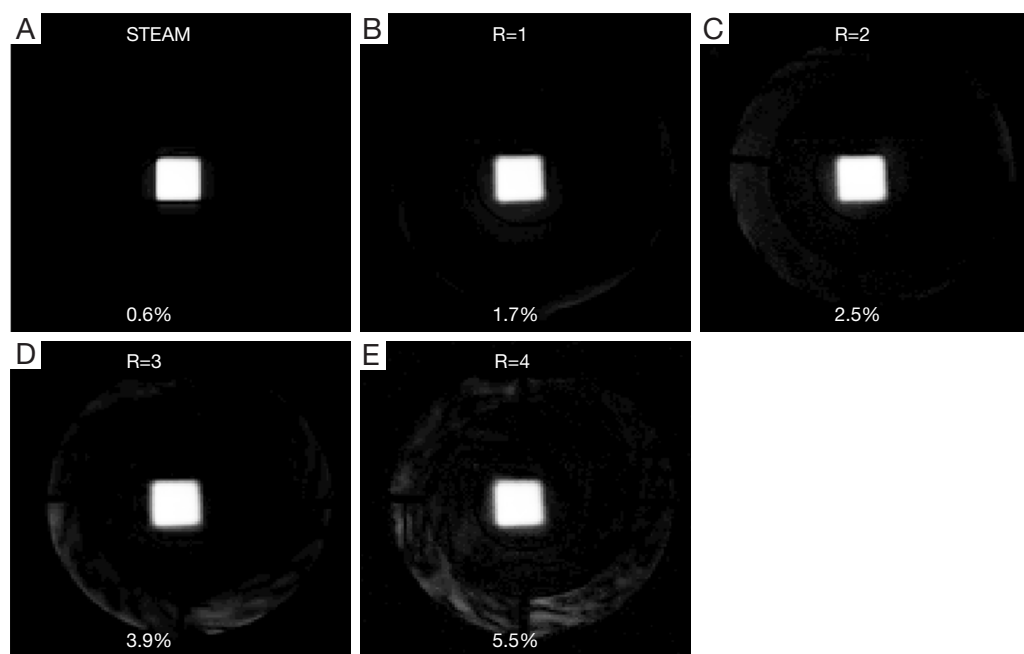


Figure 4 Reference STEAM localization image (A) and spin echo localization images for segmented 2D excitation using spiral trajectory for acceleration factors of R=1 (B), R=2 (C), R=3 (D) and R=4 (E) acquired using oil-gel-metabolite phantom. Root-mean-square deviation values are shown at the bottom of the images. 2D, two-dimensional.

range, at -2.2 ppm. *Figure 3* displays the Bloch simulations for R=1, 2, 3 and 4 at 0 Hz (on-resonance) and for R=2 at off-resonance frequencies of -325 Hz (-1.1 ppm) and -650 Hz (-2.2 ppm). The root-mean-square deviation (RMSD) values between the simulated target (*Figure 2B*) and R=1, 2, 3 and 4 (0 Hz) (*Figure 3A, D, B* and *C*, respectively) were divided by the maximum value of the simulated image to qualitatively estimate the bandwidth. % RMSD values for R=1, 2, 3 and 4 were measured as 1.3%, 2%, 3.1% and 4.5% respectively. RMSD values between R=2 (0 Hz) (*Figure 3D*) and R=2 (-325 and -650 Hz) (*Figure 3E* and *F*, respectively) were divided by the ratio of transverse to longitudinal magnetization. For R=2 (-325 Hz), the trajectory showed 1.6% RMSD and a 4.8% decrease in signal amplitude compared to R=2 (0 Hz). For R=2 (-650 Hz), 3.7% RMSD and a 9.8% decrease in signal amplitude compared to R=2 (0 Hz) were observed. Spatial localization images for the reference STEAM and the 2D selective voxel in axial orientation are shown in *Figure 4*. The RMSD values between the simulated target (*Figure 2B*) and the localization images (*Figure 4A-E*) were divided by the maximum value of the localization image. STEAM localization produced the lowest RMSD (0.6%), which indicates excellent suppression of the signal outside the voxel by gradient spoiling. In the case of segmented 2D excitation,

% RMSD values for measured images for R=1, 2, 3 and 4 were 1.7%, 2.5%, 3.9% and 5.5%, respectively. Increasing acceleration factors (R=3 and R=4) resulted in increased contamination outside the target due to undersampling of the trajectory. Therefore, fat saturation bands were employed in further *in vivo* experiments to avoid any potential contamination of spectra from residual fat signal due to insufficient outer volume suppression.

In vivo experiments

In vivo B1 maps (flip angle and phase) for the eight transmit channels in axial orientation are shown in *Figure 5*. The radial geometry of the coil provided distinct B1 profiles for each channel in the xy plane. Combined *in vivo* B1 maps corresponding to the local RF shim mode (used for water suppression pulses and refocusing pulse), CP excitation mode and the global RF shim mode (used for fat saturation pulses) are shown in *Figure 6*. *Figure 7A* shows the axial localizer image of the human head with the target voxel superimposed. Axial gradient echo localization images for R=1 and R=2 are shown in *Figure 7C* and *D* corresponding to the location of the measured B1 map. The RMSD values were calculated as 1.5% and 1.7% for R=1 and R=2,

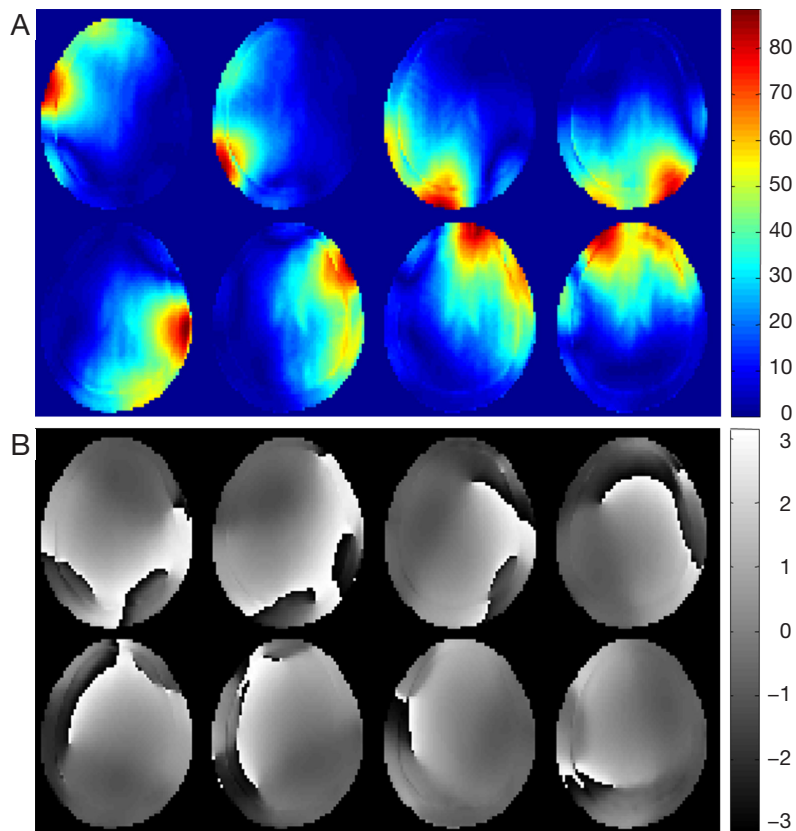


Figure 5 Flip angle ($^{\circ}$) (A) and relative phase maps (radian) (B) of the eight channel transmit coil measured *in vivo* (upper row shows coils 1 to 4 starting from left to right and lower row shows coils 5 to 8 starting from left to right).

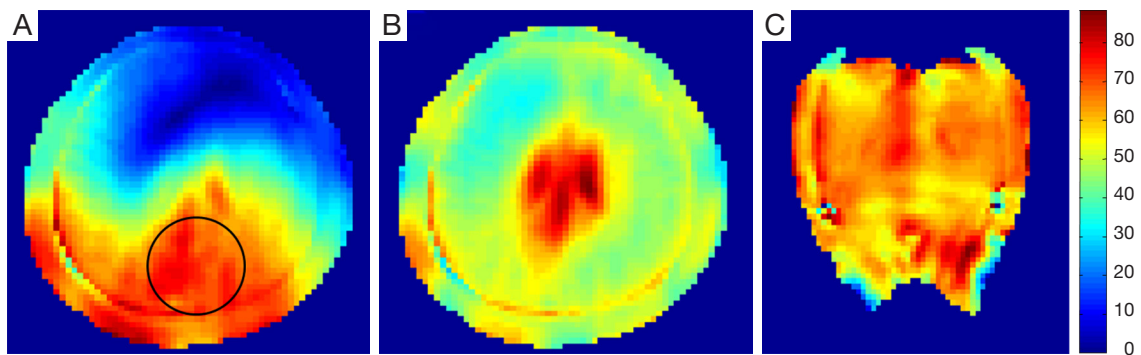


Figure 6 B1 maps demonstrating local RF shim mode used for refocusing and water suppression pulses (axial slice) (A), CP mode (axial slice) (B) and global RF shim mode used for fat saturation pulses (coronal slice) (C). CP, circularly polarized; RF, radio frequency.

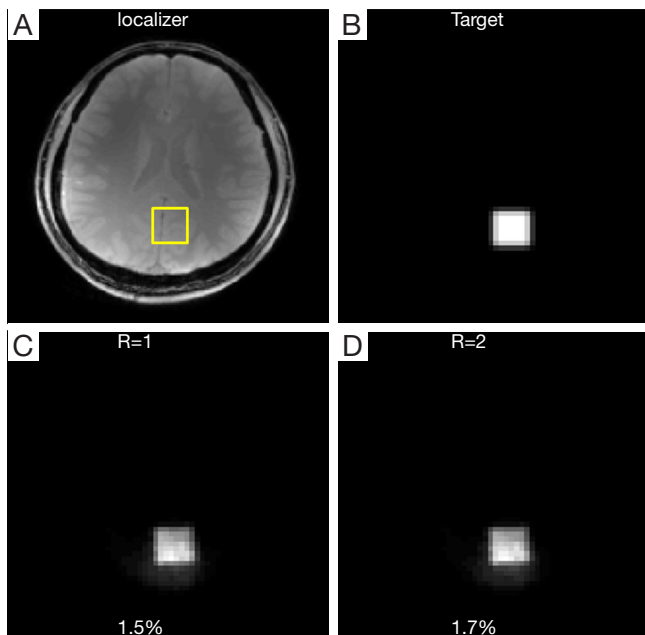


Figure 7 Axial GRE image of the brain displaying the location of excitation target in yellow (A), simulated spatial target pattern (B) and low flip angle GRE localization images for acceleration factors of R=1 (C) and R=2 (D) from 3D datasets. Root-mean-square deviation values are shown at the bottom of the images. GRE, gradient echo.

respectively. *In vivo* spectra from the reference STEAM voxel and 2D selective voxel (for R=1 and R=2) are shown in *Figure 8A-C*, respectively, along with the LCModel fits. Standard deviation values corresponding to Cramér-Rao lower bounds (CRLBs) below 20% for choline (Cho), creatine (Cr), phosphocreatine (PCr), glutamate (Glu), glutamine (Gln), glutathione (GSH) and N-acetylaspartate (NAA) are labeled at the peak locations of the reference STEAM and 2D selective MRS spectra. SNRs of the spectra were calculated as a ratio of the peak signal (NAA) to the standard deviation of noise. The reference STEAM spectrum resulted in the highest SNR of 199. SNRs of the 2D selective MRS spectra for R=1 and R=2 were 131 and 82, respectively.

Discussion

The potential of pTX to reduce the number of excitation k-space trajectory segments for 2D selective MRS by undersampling the trajectory has been explored for *in vivo* human brain MRS at 7 T. A rectangular voxel was excited by segmented 2D RF pulses and spatial selectivity was

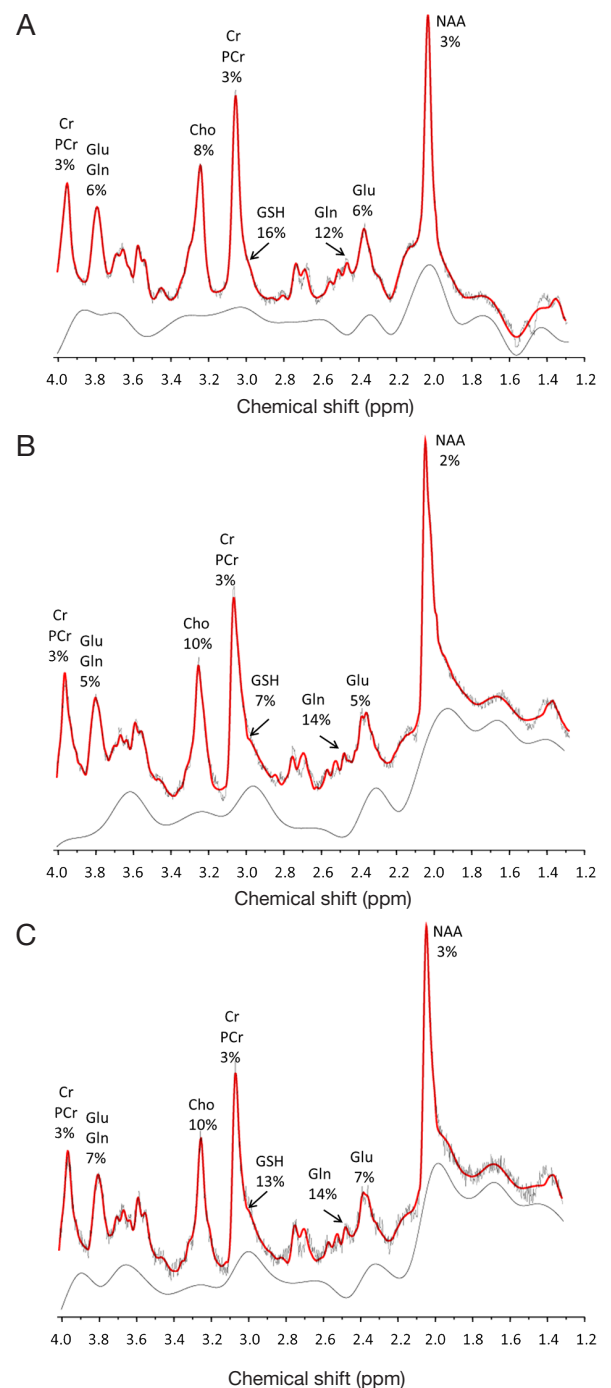


Figure 8 *In vivo* spectra for reference STEAM (A) and 2D selective MRS for acceleration factors of R=1 (B), and R=2 (C) along with LCModel fits. Metabolites with CRLBs less than 20% are labeled at the peak locations. Cho, choline; Cr, creatine; PCr, phosphocreatine; Glu, glutamate; Gln, glutamine; GSH, glutathione; NAA, N-acetylaspartate; MRS, magnetic resonance spectroscopy; 2D, two-dimensional; CRLBs, Cramér-Rao lower bounds.

compared with that of the reference STEAM voxel. RMSD of the reference STEAM voxel was compared with that of the 2D selective voxel in a phantom at different acceleration factors ($R=1, 2, 3, 4$). Localization using segmented 2D RF pulses provided very good suppression of the signal outside the target voxel for $R=1$ and $R=2$ (RMSD 1.7% and 2.5%, respectively). However, STEAM outperformed the segmented 2D excitation with 0.6% RMSD. Increased contamination was observed in the case of $R=3$ and $R=4$ (RMSD 3.9% and 5.5%, respectively) due to undersampling of the trajectory. Spiral projection artifacts start to become visible in the case of $R=3$ (Figure 3B) and $R=4$ (Figure 3C). Bloch simulations of the target pattern at off-resonance frequencies proved that segmented 2D RF pulses using a spiral trajectory provided sufficient bandwidth at 7 T (RMSD 3.7% at -650 Hz), although increased blurring of target edges is evident at -650 Hz off-resonance. *In vivo* spectra were acquired from the anterior part of the posterior cingulate cortex (pCC) of the brain with the standard STEAM and 2D selective MRS at acceleration factors of $R=1$ and 2. Relative quantification analysis of both methods detected seven major metabolites of interest (Cho, Cr, PCr, Glu, Gln, GSH and NAA) with sufficient fitting accuracy (CRLBs $<20\%$). Baseline deviation seen in the spectra of 2D selective MRS is caused possibly due to inadequate water suppression as compared to STEAM. 2D selective MRS reduced the minimum TE to 9.5 ms compared to the shortest possible TE of 15 ms with STEAM. Although, hypothetically higher SNR is expected for 2D selective MRS, limitation of RF power restricted the maximum achievable flip angle of segmented 2D RF pulses to 30° compared to 90° of standard STEAM excitation, resulting in SNR reduction for 2D selective MRS spectra (SNR 131 and 82 for $R=1$ and 2, respectively) compared to the reference STEAM spectrum (SNR 199). Twofold acceleration of trajectory for 2D selective MRS resulted in further reduction of SNR by approximately a factor of the square root of 2 (SNR 82 for $R=2$) in comparison with the unaccelerated case (SNR 131 for $R=1$).

STEAM was chosen as the reference method for comparison with 2D selective MRS as it provides better localization than PRESS. Truncated sinc pulses produce variation in the slice profile, which is especially strong in the case of the 180° refocusing pulses used twice in PRESS. As a result, the PRESS voxel no longer has a cuboid shape, and the actual volume selected by PRESS is approximately 65% smaller than that of STEAM (25). The shortest possible TE in the case of STEAM is 15 ms. PRESS uses two 180°

refocusing pulses, in addition to a 90° excitation pulse. Due to longer pulse lengths of the refocusing pulses and their associated crusher gradients, the shortest possible TE in the case of PRESS is 30 ms. Therefore, PRESS offers a twofold gain in signal intensity over STEAM only at longer TEs (>30 ms) (25).

Extra-cranial fat in the head can lead to contamination of spectra because of the very high sensitivity of lipid resonances to any spurious excitation (they are typically hundreds of times more sensitive than metabolites), thereby complicating the quantification of underlying metabolites. Therefore, 2D selective MRS requires a robust fat saturation technique to avoid intense lipid resonances in the spectra. We used four globally RF shimmed spatial pre-saturation bands to suppress extra-cranial fat, which is the most commonly used fat saturation technique. In order to reduce RF power, a single low-powered fat saturation pulse can be RF shimmed to create a ring-shaped B1 distribution mimicking head geometry (26) and subsequent crushing of the fat signal by crusher gradients.

A slight shear distortion observed in the rectangular target measured for the segmented 2D RF pulses may be due to gradient-induced excitation k-space trajectory deviations, which could be corrected by measuring the actual trajectory and incorporating it into the RF pulse design algorithm to calculate corrected RF pulses (27). Although this study was performed using a segmented spiral trajectory, it can be extended to other segmented trajectories such as radial and echo planar (10).

MRS requires excellent B0 shim over the localized area to achieve efficient water suppression, decrease chemical shift displacement artifacts and acquire spectra with narrow line widths for increased spectral resolution. It is easier to optimize the B0 field homogeneity for single voxel MRS than for 2D selective MRS as the localized area (voxel) is small. For 2D selective MRS, the B0 field over an entire 2D FOV needs to be optimized. Inhomogeneous shim outside the target would cause spurious excitation, leading to degraded water suppression and contamination of the spectra from extra-cranial lipids. In order to make RF pulses robust against B0 inhomogeneity, the existing algorithm for designing single shot RF pulses incorporating B0 map-based off-resonance correction can be adapted for designing segmented RF pulses with off-resonance correction within STA (28).

SAR management is one of the major concerns for *in vivo* application of pTX. The current implementation of the 2D selective MRS sequence is restricted by minimum achievable TR of 8 s because of conservative RF power

limits in order to comply with SAR. Further investigations are required to determine appropriate SAR estimates not only for safety reasons but to be able to optimize the sequence in the future. Determination of individual SAR estimates for each module (water suppression, fat saturation, excitation and refocusing) as a fraction of total SAR and the influence of applied RF shimming regimes on SAR would help reduce the TR and total acquisition time and increase the flip angle of segmented 2D RF pulses resulting in better SNR. This would also help optimize other full signal techniques such as PRESS, semi-LASER (29) and SPECIAL (30) and enable their direct comparison with 2D selective MRS.

Conclusions

In conclusion, we have evaluated the 2D selective MRS method both in phantom and human brain at 7 T. The method was applied both in conjunction with pTX and without pTX and compared with the standard STEAM. Different RF shim settings were used in the sequence for different RF pulses. The method offers very good spatial and spectral selectivity, although STEAM results in better outer volume suppression and SNR. Seven major metabolites of interest were reliably quantified from single voxel spectra acquired using 2D selective MRS with and without pTX and showed very good agreement with the reference STEAM spectrum. Potential improvement of SNR is expected after efficient SAR management to be implemented in the future.

Acknowledgements

The authors thank Dr. Hans-Peter Fautz for providing the B1 mapping sequence and Dr. Samir Mulla-Osman for phantom construction. This work was carried out with financial support from the INUMAC project (Grant No. 13N9208) funded by the German Federal Ministry of Education and Research (BMBF).

Authors' contributions: Gopesh Patel designed the overall study, implemented the pulse sequences and wrote the manuscript. Martin Haas designed and implemented the RF pulse design tool. Niravkumar Darji carried out experiments together with Gopesh Patel. Oliver Speck acquired the funding, revised the manuscript for critical intellectual content and provided the final approval to publish the manuscript.

Disclosure: The authors declare no conflict of interest.

References

1. Pauly J, Nishimura D, Macovski A. A k-space analysis of small tip angle excitation. *J Magn Reson* 1989;81:43-56.
2. Frahm J, Merboldt KD, Hänicke W. Localized proton spectroscopy using stimulated echoes. *J Magn Reson* 1987;72:502-8.
3. Bottomley PA. Spatial localization in NMR spectroscopy in vivo. *Ann N Y Acad Sci* 1987;508:333-48.
4. Qin Q, Gore JC, Does MD, Avison MJ, de Graaf RA. 2D arbitrary shape-selective excitation summed spectroscopy (ASSESS). *Magn Reson Med* 2007;58:19-26.
5. Pauly J, Nishimura D, Macovski A. A linear class of large-tip-angle selective excitation pulses. *J Magn Reson* 1989;82:571-87.
6. Weber-Fahr W, Busch MG, Finsterbusch J. Short-echo-time magnetic resonance spectroscopy of single voxel with arbitrary shape in the living human brain using segmented two-dimensional selective radiofrequency excitations based on a blipped-planar trajectory. *Magn Reson Imaging* 2009;27:664-71.
7. Finsterbusch J, Busch MG. Segmented 2D-selective RF excitations with weighted averaging and flip angle adaptation for MR spectroscopy of irregularly shaped voxel. *Magn Reson Med* 2011;66:333-40.
8. Katscher U, Börnert P. Parallel RF transmission in MRI. *NMR Biomed* 2006;19:393-400.
9. Zhu Y. Parallel excitation with an array of transmit coils. *Magn Reson Med* 2004;51:775-84.
10. Snyder J, Haas M, Hennig J, Zaitsev M. Selective excitation of two-dimensional arbitrarily shaped voxels with parallel excitation in spectroscopy. *Magn Reson Med* 2012;67:300-9.
11. Ullmann P, Junge S, Wick M, Seifert F, Ruhm W, Hennig J. Experimental analysis of parallel excitation using dedicated coil setups and simultaneous RF transmission on multiple channels. *Magn Reson Med* 2005;54:994-1001.
12. Grissom W, Yip CY, Zhang Z, Stenger VA, Fessler JA, Noll DC. Spatial domain method for the design of RF pulses in multicoil parallel excitation. *Magn Reson Med* 2006;56:620-9.
13. Yip CY, Fessler JA, Noll DC. Iterative RF pulse design for multidimensional, small-tip-angle selective excitation. *Magn Reson Med* 2005;54:908-17.
14. Börnert P, Aldefeld B. On spatially selective RF excitation and its analogy with spiral MR image acquisition.

- MAGMA 1998;7:166-78.
15. Van de Moortele PF, Akgun C, Adriany G, Moeller S, Ritter J, Collins CM, Smith MB, Vaughan JT, Uğurbil K. B(1) destructive interferences and spatial phase patterns at 7 T with a head transceiver array coil. *Magn Reson Med* 2005;54:1503-18.
 16. Fautz HP, Vogel M, Gross P, Kerr A, Zhu Y. B1 Mapping of Coil Arrays for Parallel Transmission. Proceedings of the 16th Scientific Meeting, ISMRM; Toronto, 2008:1247.
 17. Setsompop K, Wald LL, Alagappan V, Gagoski BA, Adalsteinsson E. Magnitude least squares optimization for parallel radio frequency excitation design demonstrated at 7 Tesla with eight channels. *Magn Reson Med* 2008;59:908-15.
 18. Deniz CM, Brown R, Lattanzi R, Alon L, Sodickson DK, Zhu Y. Maximum efficiency radiofrequency shimming: Theory and initial application for hip imaging at 7 tesla. *Magn Reson Med* 2013;69:1379-88.
 19. Ogg RJ, Kingsley PB, Taylor JS. WET, a T1- and B1-insensitive water-suppression method for in vivo localized 1H NMR spectroscopy. *J Magn Reson B* 1994;104:1-10.
 20. Wilm BJ, Svensson J, Henning A, Pruessmann KP, Boesiger P, Kollias SS. Reduced field-of-view MRI using outer volume suppression for spinal cord diffusion imaging. *Magn Reson Med* 2007;57:625-30.
 21. Provencher SW. Estimation of metabolite concentrations from localized in vivo proton NMR spectra. *Magn Reson Med* 1993;30:672-9.
 22. Young K, Govindaraju V, Soher BJ, Maudsley AA. Automated spectral analysis I: formation of a priori information by spectral simulation. *Magn Reson Med* 1998;40:812-5.
 23. Govindaraju V, Young K, Maudsley AA. Proton NMR chemical shifts and coupling constants for brain metabolites. *NMR Biomed* 2000;13:129-53.
 24. Collins CM, Wang Z, Smith MB. eds. A conservative method for ensuring safety within transmit arrays. Proceedings of the 15th joint scientific meeting. International Society for Magnetic Resonance in Medicine - European Society for Magnetic Resonance in Medicine and Biology; Berlin 2007.
 25. Moonen CT, von Kienlin M, van Zijl PC, Cohen J, Gillen J, Daly P, Wolf G. Comparison of single-shot localization methods (STEAM and PRESS) for in vivo proton NMR spectroscopy. *NMR Biomed* 1989;2:201-8.
 26. Hetherington HP, Avdievich NI, Kuznetsov AM, Pan JW. RF shimming for spectroscopic localization in the human brain at 7 T. *Magn Reson Med* 2010;63:9-19.
 27. Wu X, Vaughan JT, Uğurbil K, Van de Moortele PF. Parallel excitation in the human brain at 9.4 T counteracting k-space errors with RF pulse design. *Magn Reson Med* 2010;63:524-9.
 28. Waxmann T, Lindel TD, Seifert F, Ittermann B, Mekle R. Improved off-resonance correction for segmented spatially selective excitation pulses to achieve large excitation bandwidth. Proceedings of the 21st scientific meeting, International Society for Magnetic Resonance in Medicine; Salt Lake City 2013.
 29. Scheenen TW, Heerschap A, Klomp DW. Towards 1H-MRSI of the human brain at 7T with slice-selective adiabatic refocusing pulses. *MAGMA* 2008;21:95-101.
 30. Mekle R, Mlynárik V, Gambarota G, Hergt M, Krueger G, Gruetter R. MR spectroscopy of the human brain with enhanced signal intensity at ultrashort echo times on a clinical platform at 3T and 7T. *Magn Reson Med* 2009;61:1279-85.

Cite this article as: Patel G, Haas M, Darji N, Speck O. Evaluation of 2D spatially selective MR spectroscopy using parallel excitation at 7 T. *Quant Imaging Med Surg* 2015;5(3):344-355. doi: 10.3978/j.issn.2223-4292.2015.03.05